



AFRL-RX-WP-TP-2014-0139

**DEFECTS IN CERAMIC MATRIX COMPOSITES AND
THEIR IMPACT ON ELASTIC PROPERTIES
(POSTPRINT)**

**George J. Jefferson
AFRL/RXLN**

**JULY 2013
Interim Report**

Approved for public release; distribution unlimited.

See additional restrictions described on inside pages

STINFO COPY

© 2013 Elsevier Ltd.

**AIR FORCE RESEARCH LABORATORY
MATERIALS AND MANUFACTURING DIRECTORATE
WRIGHT-PATTERSON AIR FORCE BASE, OH 45433-7750
AIR FORCE MATERIEL COMMAND
UNITED STATES AIR FORCE**

NOTICE AND SIGNATURE PAGE

Using Government drawings, specifications, or other data included in this document for any purpose other than Government procurement does not in any way obligate the U.S. Government. The fact that the Government formulated or supplied the drawings, specifications, or other data does not license the holder or any other person or corporation; or convey any rights or permission to manufacture, use, or sell any patented invention that may relate to them.

This report was cleared for public release by the USAF 88th Air Base Wing (88 ABW) Public Affairs Office (PAO) and is available to the general public, including foreign nationals.

Copies may be obtained from the Defense Technical Information Center (DTIC)
(<http://www.dtic.mil>).

AFRL-RX-WP-TP-2014-0139 HAS BEEN REVIEWED AND IS APPROVED FOR
PUBLICATION IN ACCORDANCE WITH ASSIGNED DISTRIBUTION STATEMENT.

//Signature//

GEORGE J. JEFFERSON
Composite Performance and Application Section
Composites Branch

//Signature//

MICHAEL J. KINSELLA, Chief
Composites Branch
Structural Materials Division

//Signature//

TIMOTHY J. SCHUMACHER, Chief
Structural Materials Division
Materials and Manufacturing Directorate

This report is published in the interest of scientific and technical information exchange, and its publication does not constitute the Government's approval or disapproval of its ideas or findings.

REPORT DOCUMENTATION PAGE				Form Approved OMB No. 074-0188	
Public reporting burden for this collection of information is estimated to average 1 hour per response, including the time for reviewing instructions, searching existing data sources, gathering and maintaining the data needed, and completing and reviewing this collection of information. Send comments regarding this burden estimate or any other aspect of this collection of information, including suggestions for reducing this burden to Defense, Washington Headquarters Services, Directorate for Information Operations and Reports, 1215 Jefferson Davis Highway, Suite 1204, Arlington, VA 22202-4302. Respondents should be aware that notwithstanding any other provision of law, no person shall be subject to any penalty for failing to comply with a collection of information if it does not display a currently valid OMB control number. PLEASE DO NOT RETURN YOUR FORM TO THE ABOVE ADDRESS.					
1. REPORT DATE (DD-MM-YYYY) July 2013		2. REPORT TYPE Interim		3. DATES COVERED (From – To) 29 February 2012 – 27 June 2013	
4. TITLE AND SUBTITLE DEFECTS IN CERAMIC MATRIX COMPOSITES AND THEIR IMPACT ON ELASTIC PROPERTIES (POSTPRINT)				5a. CONTRACT NUMBER FA8650-12-C-5108	
				5b. GRANT NUMBER	
				5c. PROGRAM ELEMENT NUMBER 65502F	
6. AUTHOR(S) (see back)				5d. PROJECT NUMBER 3005	
				5e. TASK NUMBER	
				5f. WORK UNIT NUMBER X0DC	
7. PERFORMING ORGANIZATION NAME(S) AND ADDRESS(ES) (see back)				8. PERFORMING ORGANIZATION REPORT NUMBER	
9. SPONSORING / MONITORING AGENCY NAME(S) AND ADDRESS(ES) Air Force Research Laboratory Materials and Manufacturing Directorate Wright Patterson Air Force Base, OH 45433-7750 Air Force Materiel Command United States Air Force				10. SPONSOR/MONITOR'S ACRONYM(S) AFRL/RXCCP	
				11. SPONSOR/MONITOR'S REPORT NUMBER(S) AFRL-RX-WP-TP-2014-0139	
12. DISTRIBUTION / AVAILABILITY STATEMENT Approved for public release; distribution unlimited. This report contains color.					
13. SUPPLEMENTARY NOTES PA Case Number: 88ABW-2012-0462; Clearance Date: 30 January 2012. Journal article published in SciVerse Science Direct, Composites: Part B 55 (2013) 167-175. © 2013 Elsevier, Ltd. The U.S. Government is joint author of the work and has the right to use, modify, reproduce, release, perform, display or disclose the work. The final publication is available at http://dx.doi.org/10.1016/j.compositesb.2013.06.026 .					
14. ABSTRACT Defects created during the manufacture of an oxide/oxide and two non-oxide (SiC/SiNC and MI SiC/SiC) ceramic matrix composites (CMCs) were categorized as follows: (1) Intra-yarn defects such as dry fibers, (2) Inter-yarn defects such as those at crossover points, matrix voids, shrinkage cracks and interlaminar separation, and (3) Architectural defects such as layer misalignment. Their impact on elastic properties was analytically investigated using a stiffness averaging approach considering the defects to have volumetric and directional influences. In-plane tensile and shear moduli as well as the through-thickness compressive modulus were experimentally evaluated. Results of analytical model were around 7% on average from the mean value of the experimental data. It was observed that interlaminar separation drastically reduced the through-thickness modulus by about 63% for the SiC/SiNC, 40% for the MI SiC/SiC and around 32% for the oxide/oxide composites. Shrinkage cracks in oxide/oxide composite reduced the inplane tensile and shear moduli by 14% and 8.8%, respectively.					
15. SUBJECT TERMS ceramic matrix composites, elasticity, analytical modeling, mechanical testing					
16. SECURITY CLASSIFICATION OF:			17. LIMITATION OF ABSTRACT SAR	18. NUMBER OF PAGES 13	19a. NAME OF RESPONSIBLE PERSON (Monitor) George J. Jefferson
a. REPORT Unclassified	b. ABSTRACT Unclassified	c. THIS PAGE Unclassified			19b. TELEPHONE NUBER (include area code) (937) 255-1307

REPORT DOCUMENTATION PAGE Cont'd

6. AUTHOR(S)

G. Jefferson (Materials and Manufacturing Directorate), Air Force Research Laboratory)
Y. Gowayed (Department of Polymer and Fiber Engineering, Auburn University)
G. Ojard and E. Prevost (Pratt & Whitney)
U. Santhosh (Structural Analytics, Inc.)

7. PERFORMING ORGANIZATION NAME(S) AND ADDRESS(ES)

AFRL/RXCCP
Air Force Research Laboratory
Materials and Manufacturing Directorate
Wright-Patterson Air Force Base, OH 45433-7750

Department of Polymer and Fiber Engineering
Auburn University
Auburn, AL 36830

Pratt & Whitney
East Hartford, CT 06108

Structural Analytics, Inc.,
Carlsbad, CA 92008



Defects in ceramic matrix composites and their impact on elastic properties



Y. Gawayed^{b,*}, G. Ojard^c, E. Prevost^c, U. Santhosh^d, G. Jefferson^a

^a Air Force Research Laboratory, AFRL/RXLN, Wright-Patterson AFB, OH, United States

^b Department of Polymer and Fiber Engineering, Auburn University, Auburn, AL, United States

^c Pratt & Whitney, East Hartford, CT, United States

^d Structural Analytics, Inc., Carlsbad, CA, United States

ARTICLE INFO

Article history:

Received 30 July 2012

Received in revised form 28 May 2013

Accepted 12 June 2013

Available online 27 June 2013

Keywords:

A. Ceramic matrix composites

B. Elasticity

C. Analytical modeling

D. Mechanical testing

ABSTRACT

Defects created during the manufacture of an oxide/oxide and two non-oxide (SiC/SiNC and MI SiC/SiC) ceramic matrix composites (CMCs) were categorized as follows: (1) Intra-yarn defects such as dry fibers, (2) Inter-yarn defects such as those at crossover points, matrix voids, shrinkage cracks and interlaminar separation, and (3) Architectural defects such as layer misalignment. Their impact on elastic properties was analytically investigated using a stiffness averaging approach considering the defects to have volumetric and directional influences. In-plane tensile and shear moduli as well as the through-thickness compressive modulus were experimentally evaluated. Results of analytical model were around 7% on average from the mean value of the experimental data. It was observed that interlaminar separation drastically reduced the through-thickness modulus by about 63% for the SiC/SiNC, 40% for the MI SiC/SiC and around 32% for the oxide/oxide composites. Shrinkage cracks in oxide/oxide composite reduced the in-plane tensile and shear moduli by 14% and 8.8%, respectively.

© 2013 Elsevier Ltd. All rights reserved.

1. Introduction

A multitude of experimental investigations have revealed the vulnerability of CMCs to strength degradation and damage upon prolonged exposure to service loads and environmental conditions, especially at a high level of porosity and in the presence of cracks typically created during manufacture (see for example, [15]). Current design and modeling approaches have been unable to improve upon our understanding of the mechanisms responsible for the onset of life-limiting damage in the presence of defects. Such lack of insight has thus far limited the acceptance of CMCs in industrial applications and without the ability to identify defects and quantify their effect on the properties of CMCs, further development of CMC liners and other engine parts would have to rely largely on expensive trial and error approaches involving high temperature, long term testing. Besides being expensive, the trial and error approach may produce components with uncertain structural life and may not fully exploit all the desirable characteristics of CMC. Thus a greater fundamental understanding of the impact of defects on the behavior of CMCs is of crucial importance for further development of these materials.

A few research activities reported in archived literature were devoted to understand the distribution of defects and their impact on the thermal and mechanical properties of CMC. Del Puglia et al. developed a strategy to model the effect of defects on thermal transport properties of a CMC [4,6]. Physical defects, such as matrix voids and cracks, were identified and categorized and the effect of each category on the thermal transport through the composite was numerically modeled. The composite under investigation was a 10 layer T300 carbon/SiC composite in which carbon fabric was impregnated using a polymer, burned in air, then infiltrated with silicon. The silicon reacted with the carbon residues forming silicon carbide. The authors proposed four types of defects for this composite system: (A) inter-fiber micro-porosity including spherical voids and cracks parallel to fiber tows, (B) trans-tow cracks running through the tows in the planes parallel to the fibers, (C) matrix cracks perpendicular to the direction of the tows and (D) matrix voids which occur at the intersection of orthogonal tows. Del Puglia et al. concluded that the dominant defects types are A and B and that both considerably degrade the thermal properties of the composite [5].

Computed tomography (CT) scanning was used to characterize matrix voids in a MI SiC/SiC composite and finite element analysis was implemented to calculate the localized stress field [1]. Multiple images of slices from a single specimen, with an average void content of 6–7%, were used to render a 3D image containing

* Corresponding author. Tel.: +1 334 844 5496; fax: +1 334 844 4068.

E-mail address: gawayya@auburn.edu (Y. Gawayed).

Nomenclature

CMC	ceramic matrix composites	r_f	fiber radius
SiNC	silicon–nitride–carbide	S_f	fiber strength
E	elastic modulus	τ	interfacial shear strength between the fiber and the matrix
G	shear modulus	L	distance between defects
K	bulk modulus		
ν	Poisson's ratio		
A_v	vector of area fraction of defects		
p	distance between yarns		
a, b	long and short diameters of the yarn elliptical cross-section		
dz	defect dimension in z direction		
df	defect dimension in fill/weft direction		
dw	defect dimension in warp direction		
V_f	fiber volume fraction		

Subscripts

fl	fiber in longitudinal direction
d	damaged
w	warp yarns
f	fill/weft yarns
m	matrix
v	voids

porosities and defects. FEA using ANSYS® and ABAQUS® were utilized to create a mesh and evaluate the effect of the defects while modeling the composite as an orthotropic homogenous material. The study concluded that small voids had a little impact on Young's modulus but caused an increase in localized stress and thus had an effect on the onset of cracks.

Peters et al. investigated the effect of voids on the elastic moduli of SiC/SiC composites made from Nicalon fibers coated with a CVI pyro-carbon coating and a CVI matrix [20]. The void volume fraction was estimated to be around $14 \pm 3\%$. Peters et al. utilized the model developed by Hashin [12] to calculate the effect of voids on the longitudinal and shear moduli as well on the transverse moduli of the composite. The effect of voids was included in the calculation of the composite properties by either reducing the modulus of the matrix, or reducing its volume fraction. They concluded that there is little influence of the voids on the in-plane longitudinal tensile modulus while a major impact was witnessed on the shear and transverse in-plane moduli of up to 60% as compared to the theoretical values of fully dense materials.

Liaw et al. analytically studied the effect of voids for metal and ceramic matrix composites by considering the composite to be an infinite solid plate with periodically distributed inhomogeneities [14]. The homogeneous average strains along the solid have periodic disturbances due to the existence of defects. Liaw et al. used Eshelby's theory to calculate the strain distribution in the composite.

It can be seen that two modeling approaches emerge out of the literature review presented above:

- (1) A homogenization approach in which the composite is modeled as a homogeneous anisotropic body with periodic [14] or non-periodic [1,20] disturbances.
- (2) A meso-volume based approach in which the composite is divided into micro-subcells. Each subcell includes a part of the preform with or without defects [5].

The homogenization approaches viewed the composite as a homogenous anisotropic body and modeled the impact of defects as disturbances to its homogeneity, neglecting the effect of the location and size of defects, with respect to the fabric preform. On the other hand, the meso-volume approach accounted for the location and size of defects as they relate to the yarn for a specific type of CMC and modeled their impact on the thermal transport properties using FEA. It correlated defects to a single yarn, but did not provide an understanding of the defect distribution and shape with respect to the fabric preform.

In this work, defects are categorized based on their location with respect to the fabric preform and the yarns for three CMCs and used to model the effect of defects on their elastic properties.

2. Materials

Three composite systems were investigated in this work:

- (1) SiC/SiNC composite comprising a non-stoichiometric SiC (CG Nicalon™) fiber, coated with boron nitride, in a matrix of silicon, nitrogen and carbon manufactured by multiple iterations of a polymer pyrolysis process. The fiber preform was a cross-ply balanced 8 harness satin weave with 24 ends per inch and 42% fiber volume fraction.
- (2) Oxide/Oxide composite comprising a Nextel™ 720 Al_2O_3 fiber, without coating, in a sol gel matrix of Alumina Silicate. This composite has a nano-porosity of 25% in the matrix for crack deflection. The fiber preform was a cross-ply balanced 8 harness satin weave with 27 ends per inch and 46% fiber volume fraction.
- (3) Melt Infiltrated in situ BN SiC/SiC composite comprising a stoichiometric SiC (Sylramic™) fiber, with an in situ boron nitride treatment (performed at NASA-GRC), and coated with a thin layer of BN. The SiC matrix is infiltrated by vapor deposition followed by slurry casting of SiC particulates and a final melt infiltration of Si. The fiber preform was a cross-ply balanced 5 harness satin weave with 20 ends per inch and 36% fiber volume fraction.

3. Experimental evaluation of mechanical properties

Three different elastic properties were experimentally evaluated for the composite systems listed above:

- (1) In-plane elastic tensile modulus was measured using tensile tests performed per NASA's Enabling Propulsion Materials (EPM) testing standards (equivalent to ASTM C1359). The elastic modulus was calculated as the slope of the stress-strain curve in the linear region. MI SiC/SiC and oxide/oxide were tested at room temperature and SiC/SiNC was evaluated at temperatures ranging from room temperature to 1100 °C.
- (2) In-plane shear modulus was determined using biaxial extensometry on samples machined out of the panels at 45° and shear analysis consistent with ASTM D3518 at room temperature. The curves were fitted in the linear range of the stress strain curve to determine the modulus.

- (3) Through-thickness compressive elastic modulus was evaluated at room temperature using a series of stacked disks in conformance with the technique developed by Ojard et al. [17]. In this experiment, each individual disk was ground flat to remove asperities and enough disks were machined for a 2.54 cm extensometer to be flagged onto the sample. Through the center of each disk a hole was machined so that a graphite rod could be inserted to hold the stack in place and eliminate disk movement during initial loading. The rod was machined short so that it would not sustain any load that could affect the measured strain. Even though the disks were machined flat, there is a typical initial compliance to the stack that had to be overcome by sufficient load. Once the linear region of the stress–strain curve was reached, stress strain data were fitted to determine the modulus.

4. Geometric categorization of defects

Micrographic images of pristine samples were taken for the three composite systems under consideration from the same plates that were mechanically tested. Areas without a matrix material or with distorted fabric architecture were considered as defects. It is important to note that each one of these images only provide a planar view of the three dimensional defects. Based on these micrographic images, defect types were categorized as follows:

- (1) Intra-yarn defects that are located inside the yarn and limited by the outer layer of fibers defining the yarn. Only one type of inter-yarn defect was identified:
 - a. *Dry fibers*: In this defect a percent of the fibers in the yarn are not coated with matrix. This defect can occur due to reasons related the yarn itself such as in the case of a yarn with a high packing factor. Such defect can also occur due to reasons related to the fabric preform when matrix infiltration path is obstructed by another yarn within the same layer or from a different layer. Fig. 1 shows a micrographic image of a SiC/SiNC composite along with a planar view showing a possible location for this type of defect.
- (2) Inter-yarn defects that are not limited to the yarn volume and may occur either outside, or inside and outside the yarn at the same time. Four different subcategories were identified:
 - a. *Defects at crossover points*: These defects are in the form of voids located under the crimped portions of the yarn at crossover points. Their width is limited by the width of the yarn and their height by the orthogonal yarn at

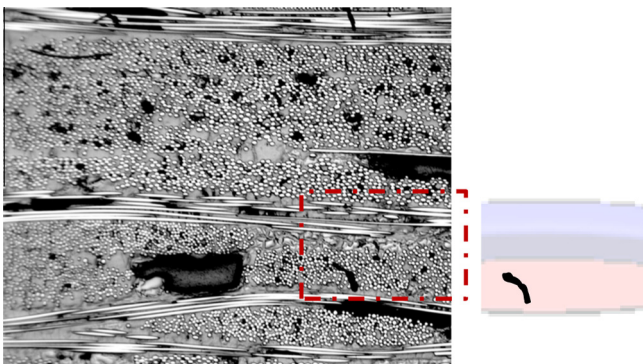


Fig. 1. Dry fibers in a micrographic image and as represented using pcGINA©. The dark object located inside the yarn in the figure on the right shows this type of defect.

the crossover point. These defects are highly affected by the architecture of the preform. For example, there are only 25 crossover points in a unit cell of a 5 harness satin weave, of which only five locations have the possibility of forming defects because this is where yarns crimp to cross over other yarns. There are four sides to each crossover location, so the maximum number of possible defects for this type is $5 \times 4 = 20$. These defects are caused due to the obstruction of the crimped yarn to the flow of the matrix material. Fig. 2 shows a micrographic image of a SiC/SiNC composite along with planar and side views showing possible locations of this type of defects.

- b. *Matrix voids*: Pockets of air and/or other gases can be entrapped in the matrix during infiltration causing voids. These voids tend to be spherical in shape and to exist in the matrix material outside the yarns. Fig. 3 shows possible locations of this type of defects in a micrographic image and a side view.
 - c. *Shrinkage cracks*: This type of defect occurs when the matrix material shrinks upon drying of the composite. The shrinkage cracks are not limited in the matrix but sometimes extend through the yarns. The micrographic images in Fig. 4 show these cracks.
 - d. *Interlaminar separation*: This type of defect occurs due to a low level of compression of layers, a kinked layer or a large air/gas pockets that may occur during manufacturing. They show in micrographic images between fabric preform layers. Fig. 5 shows the location of these defects in the micrographic images and in side and planar views.
- (3) Architectural defects that affect the preform of the layer as a whole such as:
- a. *Layer misalignment*: Misalignment of lamina can happen during hand layup of fabrics due to error in placement of preforms prior to infiltration. In this case, the cross section of the fibers in the micrographic images will not appear as a circle but rather as an ellipse.
 - b. *Fabric wrinkling*: Where the fabric may suffer wrinkling due to rough handling.

For a complete understanding of the 3D geometry of a single defect, a systematic sectioning of the composite at a constant spacing is needed to trace the exact morphology of the defect. But it also is important to remember that many defects of the same type typically show in each image revealing the change of the defect geometry along its path.

5. Analytical model of elastic properties

A model was constructed, to account for the effect of the above mentioned defects using a modified stiffness averaging technique. Stiffness averaging was selected due to the direct application of the preform geometry in its formulation and, accordingly, its ability to evaluate the effect of defects at different locations in the preform. The model takes as input stiffness of various constituents of the composite, their relative volume fraction and the volume fraction of defects in different directions. A set of analytical relationships, detailed in [19], use these parameters to evaluate the stiffness matrix for each local yarn direction. These stiffness matrices are then transformed to the material global directions and averaged according to their volumetric contribution.

To ensure the overall accuracy of this approach, elastic properties calculated using this model for a hypothetical non-defective composite were compared to those calculated using the hybrid Finite Element approach (pcGINA©) reported by Gawayed et al. [9,10] and Gawayed and Barowski [8] and the difference in results for both models was within 5%.

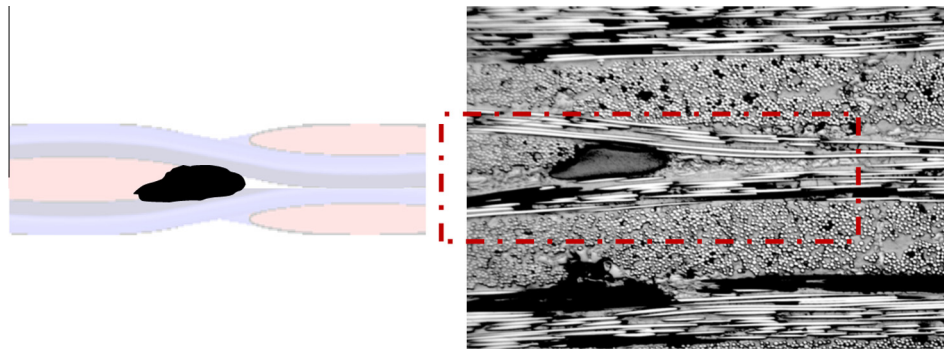


Fig. 2. Crossover defects in a micrographic image and as represented using pcGINA©. The dark object located between the crimped yarns in the figure on the left represents this type of defect.

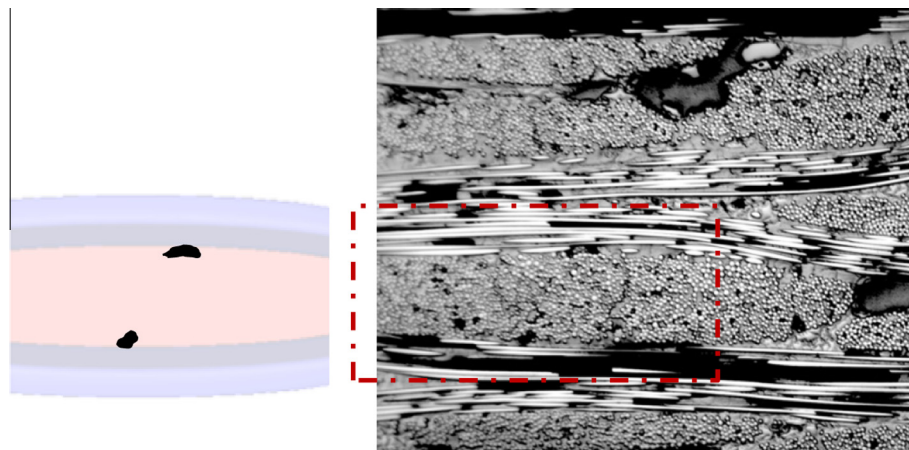


Fig. 3. Matrix voids in a micrographic image and as represented using pcGINA©. The dark shapes along the edges of the yarn in the figure on the left represent this type of defect.

The stiffness averaging approach divides the composite into a group of yarn elements, in which each element is assumed to consist of thousands of coated fibers with the matrix material surrounding each fiber. These yarn elements have lengths and directions that satisfy the geometry of the fabric (i.e., volume fraction and angle of inclination for each yarn segment). Elastic prop-

erties of the composites are calculated as follows: (i) Calculate the stiffness properties of each yarn element with respect to its local orthogonal axis system (1, 2, 3) in which axis 1 is typically parallel to the fiber/yarn longitudinal axis, (ii) rotate the local stiffness matrices in space to evaluate their stiffness with reference to the composite axis system (x, y, z), in which in this work, x is parallel to the warp direction (which is typically oriented along the length of a tensile specimen) and y is parallel to the fill direction (which is typically oriented in the short direction of a tensile specimen in the same plane as the warp yarns), and (iii) Average the stiffness matrix of all the rotated yarn elements with respect to their relative fiber volume fraction in the composite. Details of this model can be found in the work by Pastore and Gawayed [19].

Although each category of defects outlined above has its own directional nature, as it relates to the fabric architecture, all categories typically show large dimensional variability. In other words, their spatial orientation is predictable, but their spatial dimension in a particular direction is not. Accordingly, the impact of defects on elastic properties was taken as: (i) volumetric by the reduction in matrix volume, as well as, (ii) directional by including the effect of the projection of the defect along each direction.

For defects with a clear directional nature (i.e., dry fibers, crossover points, shrinkage cracks and interlaminar separation), two types of unidirectional yarn elements are identified: a non-defective and a defective element. The elastic properties of the non-defective element are calculated following the typical procedure of the stiffness averaging technique, while those for the defective element are calculated based on: (i) including the volume of defects in calculating the volume fraction of the matrix and (ii) using the vector of

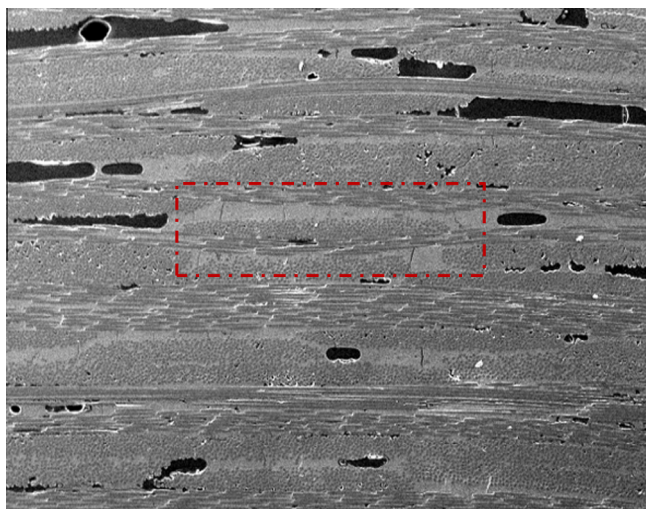


Fig. 4. shrinkage cracks in oxide/oxide composites. Notice the almost vertical cracks enclosed in the dotted box in the image.

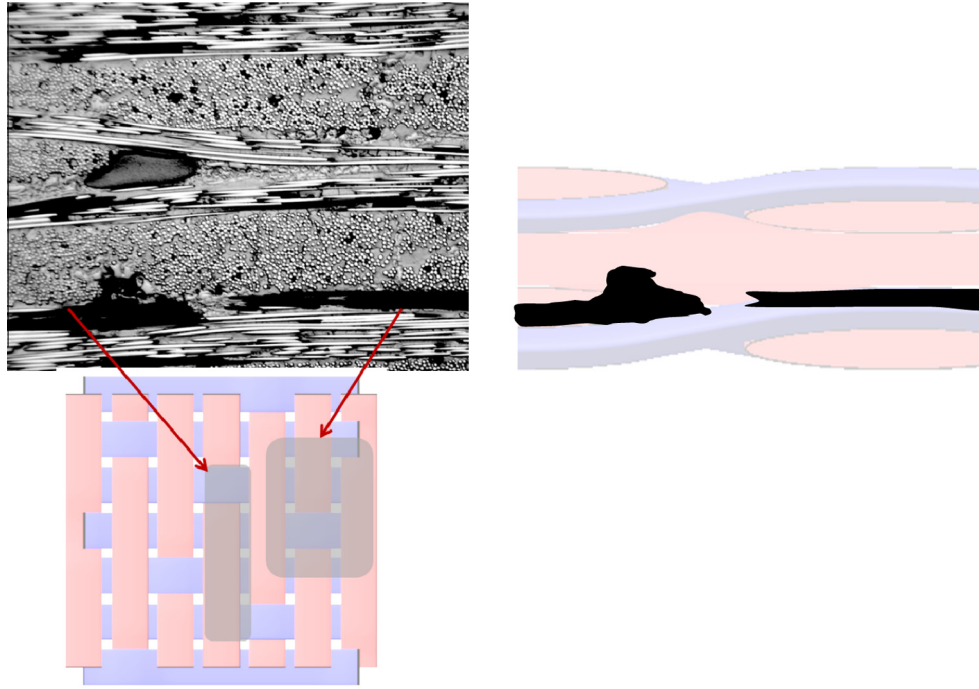


Fig. 5. Interlaminar separation defects in a micrographic image and as represented using pcGINA©. The dark objects located above the crimped yarn in the figure on the right represent this type of defect. The bottom figure show possible locations of this defect in the planar view.

the area projections to reduce the value of the moduli. Based on this approach, the equations for the three elastic (E_{id}) and three shear (G_{ijd}) moduli ($i, j = 1, 2, 3$ and $i \neq j$) for defective unidirectional elements are shown in Eq. (1), where for the local yarn axis system (1, 2, 3), axis 1 is in the longitudinal direction of the unidirectional yarn element, and axes 2 and 3 are orthogonal to 1:

$$\begin{aligned} E_{id} &= E_i(1 - Av_i) \\ G_{ijd} &= G_{ij}\left(1 - \frac{Av_i + Av_j}{2}\right) \end{aligned} \quad (1)$$

where E_i and G_{ij} ($i, j = 1, 2, 3$ and $i \neq j$) are the elastic and shear moduli of the non-defective unidirectional element, and Av_i ($i = 1, 2, 3$) are the area fraction of the defects on a plane perpendicular to axis i (i.e., area of defects divided by the total area). The volume of defects is taken into consideration by reducing the volume of the matrix.

The vector of area fraction of defects (Av_i) will change from one defect type to another based on the geometric characteristic of each defect. Table 1 provides schematic drawings for the defects and the equations used to calculate the vector of area fractions for a yarn in the warp direction. For the local axis system (1, 2, 3), the 1 axis is in along the fiber/yarn longitudinal axis, and axes 2 and 3 are orthogonal to 1. For the global axis system (x, y, z) shown in Table 1, the x axis is in the warp direction, the y axis is in the fill direction and z axis is in the through-thickness direction. Following the same logic, similar equations were formulated for the fill yarns in the case of balanced and unbalanced weaves.

In Table 1, a, b = long and short diameters of the yarn elliptical cross-section, respectively, w = warp and f = fill/weft directions, p_i = yarn spacing in i direction ($i = w, f$), n_i = number of ends in i direction per unit length ($i = w, f$), and df is the length of the projection of the defect in the fill direction, dw is the length of the projection of the defect in the warp direction, dz is the length of the projection of the defect in the through-thickness direction and (*) is used as a multiplication sign.

For the dry fibers defect, Eq. (1) for E_{id} is modified to include the effect of the stress-discontinuity in the fibers direction utilizing a

shear-lag model as follows, while the rest of the equations for other composite moduli remain the same:

$$E_{id} = \left(E_1 - \frac{E_f S_f V_f r_f}{4\tau(L - dw)}\right)(1 - Av_1) \quad (2)$$

where E_f is the fiber longitudinal modulus, S_f the fiber strength, V_f the fiber volume fraction, r_f the fiber radius, L the distance between defects, and τ is the interfacial shear strength between the fiber and the matrix.

Matrix voids were assumed to be spherical and to affect the elastic tensile and shear moduli of the matrix. These effects were determined utilizing the approach developed by Weng and Tandon [21,22] as shown in Eq. (3) for the effect of inclusions (r) on the bulk (K_{mv}), tensile (E_{mv}) and shear (G_{mv}) moduli of the homogeneous materials:

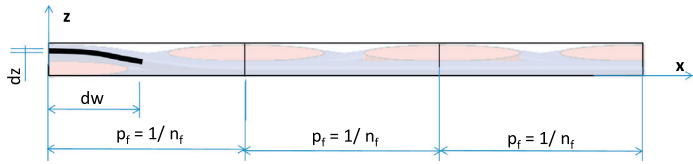
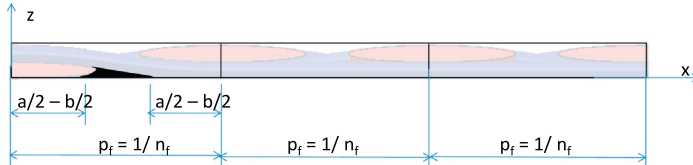
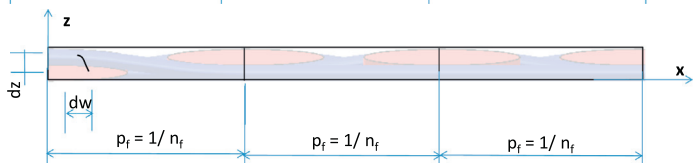
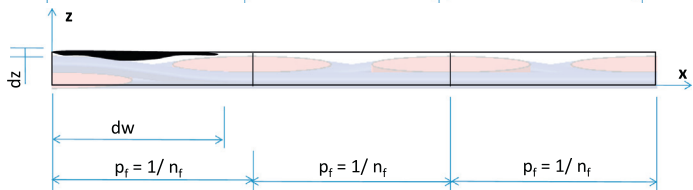
$$\begin{aligned} K_{mv} &= K_m \left(1 + \frac{a_1}{1 - \alpha a_1}\right) \\ G_{mv} &= G_m \left(1 + \frac{b_1}{1 - \beta b_1}\right) \\ E_{mv} &= 2G_{mv}(1 + \nu_m) \\ \alpha &= \frac{3k_m}{3k_m + 4G_m} \\ \beta &= \frac{6(k_m + 2G_m)}{5(3k_m + 4G_m)} \end{aligned} \quad (3)$$

For a matrix with inclusions r :

$$\begin{aligned} a_1 &= \sum_r \frac{V_r(K_r - K_m)}{\alpha(K_r - K_m) + K_m} \\ b_1 &= \sum_r \frac{V_r(G_r - G_m)}{\beta(G_r - G_m) + G_m} \end{aligned}$$

where K, G, E and ν are bulk, shear and elastic moduli and the Poisson's ratio of the matrix, respectively, V is volume fraction, m refers to matrix, r refers to inclusion, ν refers to voids, α, β, a_1 and b_1 are defined constants. The inclusion in the case of defects is assumed to be air.

Table 1
Vector of area fractions for different defect types for a yarn in the warp direction.

Defect type	Schematic of defect	Area fraction
Dry fibers		$Av_1 = \frac{dz}{2bp_w} \frac{df}{dw}$ $Av_2 = \frac{dz}{2bp_f} \frac{dw}{df}$ $Av_3 = \frac{dw}{p_w p_f} \frac{df}{dw}$
Crossover points		$Av_1 = \frac{ba}{2bp_w}$ $Av_2 = \frac{b(p_f - a + b)}{2bp_f}$ $Av_3 = \frac{a(p_f - a + b)}{p_w p_f}$
Shrinkage cracks		$Av_1 = \frac{dz}{2bp_w} \frac{df}{dw}$ $Av_2 = \frac{dz}{2bp_f} \frac{dw}{df}$ $Av_3 = \frac{dw}{p_w p_f} \frac{df}{dw}$
Interlaminar separation		$Av_1 = \frac{dz}{2bp_w} \frac{df}{dw}$ $Av_2 = \frac{dz}{2bp_f} \frac{dw}{df}$ $Av_3 = \frac{dw}{p_w p_f} \frac{df}{dw}$

In the case of lamina misalignment, by assuming that fibers have a circular cross-section, any departure from such geometric form can be used as an indicator of misalignment. The effect of layer misalignment is included by changing the orientation angle in the rotation of the stiffness matrix of the local element from the local axis system to the global composite axis system in order to match the actual angle of the layer.

6. Results

Micrographic images obtained from different samples (10 images per data point) were thresholded at the lower inflection point of the slope of the grey-scale curve. Black pixels were assumed to be defects and were manually measured and categorized.

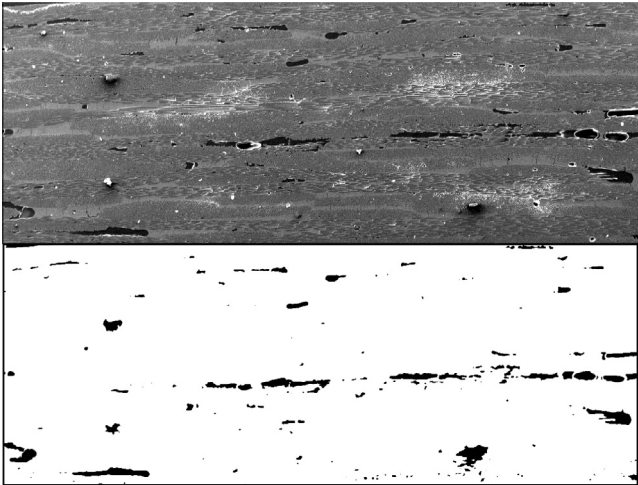


Fig. 6. Micrographic (top) and processed images (bottom) of oxide/oxide composite.

Instances of defects were categorized per defect type. For each defect type in each image, different instances were measured and results from different images were averaged. Black pixels inside the area typically occupied by the yarn and running parallel to the fibers were assumed to be fibers pulled out during polishing. Figs. 6 and 7 show examples of image processing for oxide/oxide and MI SiC/SiC composites, respectively. These thresholded images isolate the defects and allow the quantification of their area or length fractions. In both images, the large ratio of the length of the interlaminar separation defect versus the total length of the image can be

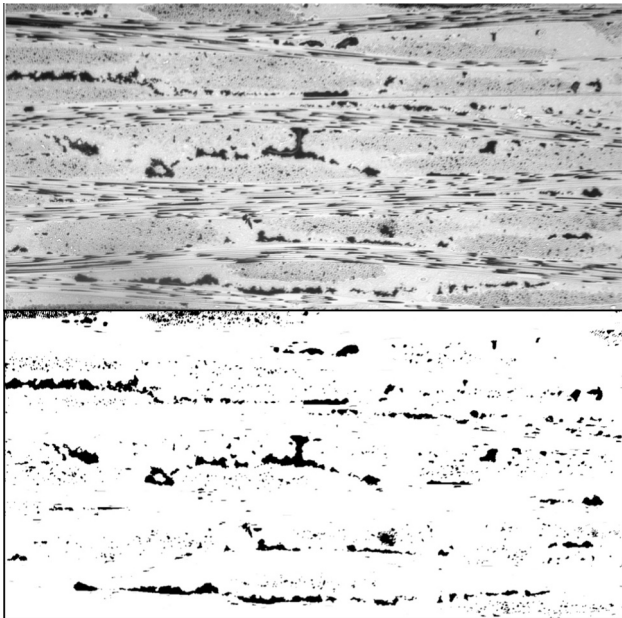


Fig. 7. Micrographic (top) and processed images (bottom) of MI SiC/SiC composite.

Table 2Vector of area fractions and volume fraction of defects (V_d) for a yarn in the warp direction^a (in percent).

		Intra-yarn	Inter-yarn			
		Dry fiber	Crossover points	Matrix voids ^b	Shrinkage cracks	Interlaminar separation
SiC/SiNC	Av_1	1.51	37.8	–	–	2.80
	Av_2	2.0	9.9	–	–	2.80
	Av_3	3.0	29.9	–	–	64.0
	V_d	2.44	4.51	2.44	–	2.86
Oxide/oxide	Av_1	0.60	0.53	–	18.0	1.55
	Av_2	0.72	2.67	–	0.30	1.55
	Av_3	1.2	1.13	–	0.06	31.9
	V_d	0.79	0.33	0.79	0.01	1.57
MI SiC/SiC	Av_1	5.04	3.15	–	–	1.58
	Av_2	4.0	1.24	–	–	1.58
	Av_3	5.04	3.12	–	–	40.0
	V_d	5.39	0.4	1.13	–	1.57

^a For the balanced fabrics discussed in this work, vectors of area fraction in the warp and fill directions are expected to be similar.^b Matrix voids were assumed to be spherical.**Table 3**

Properties of constituent materials at room temperature as used in the model (GPa).

		SiC/SiNC	Oxide/oxide	MI SiC/SiC ^h
Coated fiber	V_f	0.42 ^a	0.46 ^a	0.36 ^a
	E_{fl}	184.7 ^{b,c}	257.2 ^b	332.37 ^{b,c}
	E_{ft}	74.12 ^{b,c}	257.2 ^f	130.18 ^{b,c}
	G_f	31.20 ^d	105.1 ^d	60.05 ^d
	ν_f	0.16 ^{a,c}	0.224 ^a	0.178 ^{a,c}
Matrix	E_m	139.70 ^b	21 ^g	329.24 ^{b,c}
	G_m	58.21 ^d	8.54 ^d	139.27 ^d
	ν_m	0.20 ^e	0.23 ^e	0.182 ^e

^a Data from manufacturer.^b Nano-indentation [18].^c Calculated using Rule of Mixtures.^d Calculated using elasticity equations.^e Estimated.^f Uncoated isotropic fiber.^g Refs. [7,11] to account for growth of necks between particles via surface diffusion.^h Ref. [9].

seen. Table 2 lists the vector of area fractions and volume fraction of each defect type for the three CMCs. Shrinkage cracks were limited to oxide/oxide and no layer misalignment was observed in these images.

Additional data needed to run the analytical model include information on the preform architecture, detailed earlier in the section on materials, and the properties of the coated fiber and the matrix as listed in Table 3 at room temperature. The effect of temperature on the coated fiber for the SiC/SiNC composite is listed in Table 4. Polymer derived SiC and SiNC matrix material do not exhibit a major change in their elastic properties at temperatures below 1300 °C [3], accordingly, the matrix properties were kept constant at different temperatures.

Table 4Properties of coated SiC fiber in SiC/SiNC composite at elevated temperatures as used in model^a (GPa).

	RT	800 °C	1100 °C	1200 °C	1300 °C
E_{fl}	184.7	171.7	156.8	145.5	132.5
E_{ft}	74.12	72.4	70.2	68.4	66.0
G_f	31.20	30.5	29.6	28.8	27.9
ν_f	0.16	0.16	0.16	0.16	0.16

^a Calculated from [2,16] using rule of mixtures and elasticity equations. Poisson's ratio was assumed to remain constant.

In Table 3, E_{fl} , E_{ft} are the tensile modulus of the fiber in the longitudinal and transverse directions, respectively, G_f is the shear modulus of the fiber and ν_f is the Poisson's ratio of the fiber, E_m is the tensile modulus of the matrix, G_m is the shear modulus of the matrix, ν_m is the Poisson's ratio of the matrix and V_f is the fiber volume fraction.

Computer codes were developed utilizing the above equations using Matlab[®] to account for the effect of each defect type as a percentage of depreciation in properties. Utilizing these equations and the data in Tables 2–4, the effect of defects on the in-plane and the through-thickness moduli as well as the in-plane shear modulus were evaluated for the plates from which the defect data was obtained. The results are listed in Table 5, with at least 5 samples per data-point. Layer misalignment was not observed in these composites and accordingly their results are not reported. Table 6 shows comparison between measured data and calculated properties with the effect of defects mathematically added. The effect of temperature on the in-plane modulus of the SiC/SiNC composite is shown in Fig. 8.

7. Analysis and discussion

Utilizing the geometric categorization system for defects outlined above, work done and reported in archived literature on similar composite systems can be classified with respect to the preform architecture. For example, the work done by Abul-Aziz

Table 5

Analytical results showing percent reduction in elastic property due to defects.

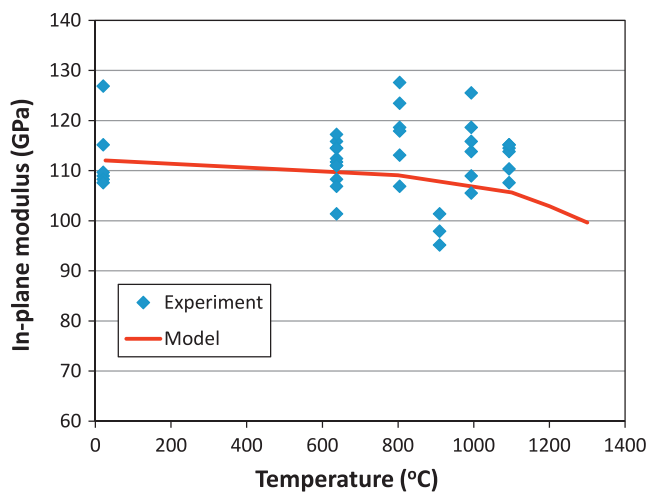
		Intra-yarn	Inter-yarn			
		Dry fiber	Crossover points	Matrix voids	Shrinkage cracks	Interlaminar separation
SiC/SiNC	E_x	2.80	3.35	3.94	–	3.51
	E_z	1.36	3.48	3.64	–	63.36
Oxide/oxide	E_x	1.84	0.13	0.44	14.05	1.36
	E_z	0.13	0.26	1.44	0.92	31.93
MI SiC/SiC	G_{xy}	0.00	0.07	1.49	8.80	0.07
	E_x	4.11	0.51	1.92	–	2.26
	E_z	2.12	0.00	1.50	–	39.61
	G_{xy}	1.20	0.38	1.42	–	0.65

Where E_x , E_z are the tensile modulus of the composite in the in-plane and through-thickness directions, respectively, and G_{xy} is the in-plane shear modulus of the composite.

Table 6

Experimental data and analytical results (GPa).

		Experimental data	Analytical results	Difference from average experimental value (%)
SiC/SiNC	E_x	112.7 ± 7.4	112.8	0.1
	E_z	31.7 ± 6.5	29.3	7.6
Oxide/oxide	E_x	71.6 ± 6.4	68.5	4.3
	E_z	33.2 ± 8.8	24.9	25.0
	G_{xy}	13.3 ± 0.6	13.3	0.0
MI SiC/SiC	E_x	254.9 ± 7.4	239.1	6.2
	E_z	130.0 ± 3.4	110.3	15.2
	G_{xy}	95.8 ± 0.6	83.4	12.9

**Fig. 8.** The effect of temperature on the in-plane modulus of cross-ply SiC/SiNC 8-layers composite.

et al. [1] on MI SiC/SiC composite includes matrix voids and crossover points, while the work done by Peters et al. [20] on CVI SiC/SiC composite only considers matrix voids. For the carbon/SiC composite reported by Puglia et al. [4,6], the A classification includes dry fibers and matrix voids, the B and C classifications are similar to shrinkage cracks and the D classification is crossover points. No record was found in archived literature on evaluating the effect of interlaminar separation, dry fibers or misaligned layers.

It is important to note that there are some limitations to the accuracy of extracting the defect data from the micrographic images. For example, interlaminar separation typically occurs at the edge of yarns. When cut along the length of the yarn, the fibers are typically pulled out as seen in Figs. 2 and 3, thus limiting the ability to identify the exact location and extent of the interlaminar separation. Also, in the case of matrix voids and dry yarns, the resolution of the images has to be high enough to allow for accurate measurement of small amount of defects/voids. The issue with image resolution is also

crucial when it comes to shrinkage cracks that require high resolution as well as high magnification in order to capture the size and distribution of the cracks.

Defect types can have different distributions in different composites as shown in Table 2. Dry fibers were highest in MI SiC/SiC followed by SiC/SiNC and lowest in the oxide/oxide. Defects at crossover points were mainly present in SiC/SiNC composites. Matrix voids were highest in SiC/SiNC and much lower in the other two composites. The effect of interlaminar separation was more significant when considering separation area rather than separation volume. SiC/SiNC had the highest separation area followed by the MI SiC/SiC and oxide/oxide composites.

Defects were prevalent in SiC/SiNC composites than other systems. This is, most probably, due to the iterative pyrolysis steps used during manufacture and the shrinkage associated with each step. Pyrolysis of preceramic polymers causes them to remarkably shrink. This is one of the drawbacks of this material because cracks, even after repeated infiltrations, remain a source of stress concentration in the matrix as well as a source for reduction in thermal and mechanical properties. The shrinkage is due to two reasons: (i) Organic and inorganic groups oxidize or evaporate as well as a partial reform of the polymer structure due to crystallization, and (ii) At a very high temperature, depending on the polymer composition and the pyrolysis environment, crystallization starts and causes further shrinkage, causing a change in density [13].

Defects caused reduction in the elastic properties of the composites studied in this work. Interlaminar separation has the most pronounced effect as seen in Table 5 with a reduction of over 63% in the through-thickness modulus for SiC/SiNC, 40% for the MI SiC/SiC and around 32% for the oxide/oxide. Shrinkage cracks reduced the in-plane modulus of the oxide/oxide by about 14% and the in-plane shear by 8.8% with a negligible effect on the through-thickness modulus since the cracks are mostly vertical cracks in the out-of-pane direction. A 2.46% of matrix voids in SiC/SiNC composites caused around 4% reduction in the in-plane and through-thickness moduli. Dry fibers reduced the in-plane modulus by 4.1% in the MI SiC/SiC and 2.8% in the SiC/SiNC composites. Also, 4.51% crossover point defects in SiC/SiNC composite caused a reduction in the in-plane and

through-thickness moduli of about 3.5%. The effect of other defects was equal-to or lower-than 2% of the non-defective elastic properties. It can be concluded from these results that for the composite systems investigated in this work: (i) in-plane modulus is mainly affected by shrinkage cracks and dry fibers, (ii) through-thickness modulus is highly affected by interlaminar separation, (iii) in-plane shear modulus is mostly affected by shrinkage cracks, and matrix voids, and (iv) matrix voids and defects at crossover points affected all elastic properties by an amount dependent on their volume fraction.

It can be seen from Table 6 and Fig. 8 that model predictions are within a reasonable range from experimental data for most properties, except for the out-of-plane properties of the MI SiC/SiC composite, which was underestimated by around 15% from the experimental range of the data. Interlaminar defects play an important dynamic role in these out-of-plane properties. The regions covered by these defects will not carry tensile forces in the out-of-plane direction, while it may carry compressive stresses after experiencing a limited amount of deformation. Since the through-thickness modulus was measured by applying compression on a group of stacked disks, it is expected that its value increased with the increase in the stress level until it reaches a final plateau which can be as high as the value of a defect-free composite. A detailed discussion of the through-thickness compressive modulus of MI SiC/SiC can be found in [9].

Identifying, categorizing and quantifying defects can help improve the composite manufacturing process. For example, the shape and distribution of intra- and inter-yarn defects are typically affected by manufacturing pressure and temperature, the viscosity of the infiltrating matrix medium, shrinkage of the matrix upon cooling and the existence of rigid particulates as part of the matrix. A study of the effect of each of these manufacturing parameters is needed to correlate them to the existence and distribution of a specific defect type and allow for their reduction and eventual elimination. For example, the high value of dry fibers in MI SiC/SiC points to a limited penetration of the CVI SiC into the yarns. A modification in the manufacturing procedure can help remedy this situation. Also, shrinkage cracks are only evident in oxide/oxide because no additional matrix material is used to fill up these shrinkage cracks. In the case of SiC/SiNC composite, multiple matrix infiltration steps are used to fill up voids and cracks while in MI SiC/SiC Si metal infiltration fills up the voids.

8. Conclusions

Defects in an as-manufactured oxide/oxide and two non-oxide (SiC/SiNC and MI SiC/SiC) ceramic matrix composites were categorized and their volume fraction quantified using optical imaging and image analysis. It was observed that for most defect types the volume fraction of defects was low except for shrinkage cracks in oxide/oxide composites, crossover defects in MI SiC/SiC composite and interlaminar separation for all composites.

A stiffness averaging approach was used to quantify the effect of defects on elastic properties utilizing the value of their volume fraction. In-plane tensile and shear moduli as well as the through-thickness compressive modulus for the composite systems were experimentally evaluated and compared to results of the model. It was observed that the most affected property was

the through-thickness modulus due to interlaminar separation defect in all the composite systems. In-plane tensile and shear moduli in oxide/oxide composite were also reduced by shrinkage cracks.

Acknowledgment

The Air Force Research Laboratory, Materials & Manufacturing Directorate, Wright-Patterson AFB, OH, USA supported this effort under contract FA8650-11-M-5130.

References

- [1] Abdul Aziz A, Sauri C, Bui Xuan V, Young P. On the material characterization of a composite using micro-CT image based finite element modeling. In: Mufti Aftab A, Gyekenyesi Andrew L, Shull Peter J (editors), Proceedings of SPIE, Vol. 6176, nondestructive evaluation and health monitoring of aerospace materials, composites, and civil infrastructure V, 617605; 2006.
- [2] Bodet R, Bourrat X, Lamon J, Naslain R. Tensile creep behaviour of a silicon carbide-based fibre with a low oxygen content. *J Mater Sci* 1995(30):661–77.
- [3] Colombo P, Riedel R, Soraru G, Kleebe H (editors). Polymer derived ceramics: from nano-structure to applications. Destech Publications, Inc; 2009.
- [4] Del Puglia P, Sheikh M, Hayhurst D. Classification and quantification of initial porosity in a CMC laminate. *Composites Part A* 2004;35:223–30.
- [5] Del Puglia P, Sheikh M, Hayhurst D. Modelling the degradation of thermal transport in a CMC material due to three different classes of porosity. *Model Simul Mater Sci Eng* 2004;12:357–72.
- [6] Del Puglia P, Sheikh M, Hayhurst D. Thermal transport property prediction of a CMC laminate from base materials properties and manufacturing porosities. *Proc R Soc A* 2005;461:3575–97.
- [7] Fujita H, Jefferson G, McMeeking RM, Zok FW. Mullite–Alumina mixtures for Use as porous matrices in oxide fiber composites. *J Am Ceram Soc* 2004;87(2):261–7.
- [8] Gawayed Y, Barowski L. pcGina© software, 12; 2004.
- [9] Gawayed Y, Ojard O, Miller R, Santhosh U, Ahmad J, John R. Correlation of elastic properties of melt infiltrated SiC/SiC composites to in situ properties of constituent phases. *Compos Sci Technol* 2010;70:435–41.
- [10] Gawayed Y, Pastore C, Howarth C. Modification and application of unit cell continuum model to predict the elastic properties of textile composites. *Compos A – Appl Sci Manuf* 1996;27:149–55.
- [11] Hammond, Elzey D. Elevated temperature mechanical properties of partially sintered alumina. *Compos Sci Technol* 2004;64:1551–63.
- [12] Hashin Z. Theory of fiber reinforced materials, NASA CR-1974; 1972.
- [13] Motz G, Schmidt S, Beyer S. The PIP process: Precursors Properties and applications, chapter in Ceramic Matrix Composites: Fiber Reinforced Ceramics and their Applications, Walter Krenkel editor, Wiley-VCH Verlag GmbH & Co. KGaA; 2008.
- [14] Liaw P, Hsu D, Yu N, Miriyala N, Saini V, Jeong H. Investigation of metal and ceramic-matrix composite moduli: experiment and theory. *Acta Mater* 1996;44(5):2101–13.
- [15] Mei H, Xu Y, Cheng L, Zhang L. Nondestructive evaluation and mechanical characterization of a defect-embedded ceramic matrix composite laminate. *Int J Appl Ceram Technol* 2007;4(4):378–86.
- [16] NIST database. <http://www.ceramics.nist.gov/srd/summary/scdscs.htm> [accessed 28/3/11].
- [17] Ojard G, Barnett T, Calomino A, Gawayed Y, Santhosh U, Ahmad J, et al. Through thickness modulus (E33) of ceramic matrix composites: mechanical test method development. *Ceram Eng Sci Proc* 2007;27(2):331–8.
- [18] Ojard G, Rugg K, Colby M, Riester L, Gawayed Y. Constituent properties determination and model verification for ceramic matrix composite system. *Ceram Eng Sci Proc* 2005;26(2):343–50.
- [19] Pastore C, Gawayed Y. A self-consistent fabric geometry model: modification and application of a fabric geometry model to predict the elastic properties of textile composites. *ASTM J Compos Technol Res* 1994;16(1):32–6.
- [20] Peters P, Martin E, Pluvinage. Influence of porosity and fibre coating on engineering elastic moduli of fibre-reinforced ceramics (SiC/SiC). *Composites* 1995;26(6):108–14.
- [21] Tandon G, Weng G. Stress distribution in and around spheroidal inclusions and voids at finite concentrations. *J Appl Mech* 1986;53:511–8.
- [22] Weng G. Some elastic properties of reinforced solids with special reference to isotropic ones containing spherical inclusions. *Int J Eng Sci* 1984;22(7):845–56.